Sputter-Deposited Titanium Oxide Layers as Efficient Electron Selective Contacts in Organic Photovoltaic Devices

Mina Mirsafaei, Pia Bomholt Jensen, Mehrad Ahmadpour, Harish Lakhotiya, John Lundsgaard Hansen, Brian Julsgaard, Horst-Günter Rubahn, Remi Lazzari, Nadine Witkowski, Peter Balling, et al.

Sputter deposited titanium oxide layers as efficient electron selective contacts in organic photovoltaic devices

Mina Mirsafaei[1], Pia Bomholt Jensen[2], Mehrad Ahmadpour[1], Harish Lakhotiya[2], John Lundsgaard Hansen[2], Brian Julsgaard[2], Horst-Günter Rubahn[1], Rémi Lazzari[3], Nadine Witkowski[3], Peter Balling[2], Morten Madsen[1]*

[1] SDU NanoSYD, Mads Clausen Institute, University of Southern Denmark, Alsion 2, Sønderborg, DK-6400, Denmark

[2] Department of Physics and Astronomy/Interdisciplinary Nanoscience Center (iNano), Aarhus University, Ny Munkegade 120, DK-8000 Aarhus C, Denmark

[3] Sorbonne Université, UMR CNRS 7588, Institut des Nanosciences de Paris (INSP), 4 place Jussieu, 75005 Paris, France

KEYWORDS. Organic photovoltaics, Metal Oxide Interlayers, Titanium Oxide, S-Shape Free, Sputter Deposition

ABSTRACT. Organic photovoltaics (OPV) has recently reached power conversion efficiencies of 17.3%, making it a green technology that not only offers short energy payback times and new photovoltaic integration schemes, but also can deliver competitive power outputs. OPV typically employs electron selective contact layers made from low work function n-type metal oxide semiconductors, such as titanium oxide (TiO_2) or zinc oxide (ZnO), developed from a variety of

deposition techniques. However, in the case of TiO_2 interlayers, the appearance of unwanted s-shape characteristics has been reported extensively in the literature in the past, for a variety of different deposition method used. It has been shown that the s-shape arises from negatively charged chemisorbed oxygen, and that it can be deactivated by UV light illumination, which, however, is hardly compatible with real-life OPV application. In this work, we introduce sputtered crystalline titanium oxide layers as efficient s-shape-free electron selective extraction layers in organic solar-cell devices. We demonstrate that the onset of crystallization takes place at substrate growth temperatures of around 100°C for the TiO_x thin films, and that the crystallization onset temperature correlates well with a strong increase in device performance, and the removal of any s-shape characteristics. Optical, structural, compositional and electronic energy-level characterizations of the TiO_x layers are shown in the present work, and point to the formation of an oxide with a low surface-defect density, developed from the sputter-crystallization process. Importantly, well-functioning s-shape free PTB7:$PC_{70}BM$ devices are demonstrated for TiO_x growth temperatures of 155°C.

INTRODUCTION. Organic Photovoltaics (OPV) represent an unprecedented class of solar energy technology that offers large cost reductions for flexible panels, using potentially inexpensive materials and especially low cost printing techniques from Roll-to-Roll (R2R) processing technology[1-2]. Their lightweight, mechanical flexibility and semitransparency allow for completely new photovoltaic integration schemes, also targeting aesthetic design aspects[3]. Recently, significant improvements have been made in the power conversion efficiency (PCE) of OPV, particularly achieved through the development of new non-fullerene acceptor materials[4-5], leading to world record PCE values of 15.8% (certified) for organic single-junction solar cells[5].

The use of interfacial layers in organic solar cells has been investigated intensively over the past

years, as it has a strong impact on both the power conversion efficiency and stability of the devices[6]. For electron selective transport layers (ETL), low work function wide band gap semiconductors are required. Thin organic or hybrid ETL have been demonstrated to improve the performance of PTB7 based inverted[7] and standard[8] configuration OPV devices. Among the investigated ETL, n–type metal oxides have drawn a lot of attention due to their chemical stability, high optical transmittance and favorable energy-level alignment with many commonly used organic electron acceptor materials. To date, effective binary and ternary oxides such as ZnO[9], TiO_x[10], Nb_2O_5[11], SnO_x[12], Al-doped ZnO[13], Mg-doped ZnO[14], and Cs-doped metal oxides[15] have been investigated as ETL for organic solar cell devices. With work function values around 4.4 eV[16] and a deep lying valence band, titanium oxide (TiO_x) has been demonstrated as an efficient electron-selective contact, which has been extensively used in both standard and inverted OPV device configurations[17-19]. There are several methods available for fabricating TiO_x thin films for organic solar cells, including solution processing[10,19,20] and atomic-layer deposition[21]. However, a typical challenge when using TiO_x as electron selective contact layers, is the formation of the well-known s-shape current-voltage characteristics that lowers the initial fill factor values, and thus also the power conversion efficiency[16]. This has resulted in the need for a UV light-soaking procedure to activate the metal-oxide surface and remove the s-shape[16]. This is, however, far from ideal for real operating solar OPV modules, also since UV filters are typically employed to protect the organic active layer from UV degradation. Strategies pursued to remove the observed s-shape in TiO_x based OPV cells include chemical doping of the TiO_x layer[22] or application of thin functionalized layers to modify the surface properties of the TiO_x layer[23-24].

In the literature there is a common agreement that physisorbed oxygen from the environment

leads to negatively charged chemisorbed oxygen species in TiO_x layers, which results in the hampered charge transport properties that cause the s-shape current-voltage characteristics[25-26]. It has also been shown that the illumination with UV light leads to a neutralization of the charged oxygen species, followed by desorption of molecular oxygen and lowered TiO_x work function values[16]. The exact position of the energy barrier arising across the TiO_x interface in an OPV layer stack, as an effect from the negatively charged chemisorbed oxygen, has been debated. Kim *et al.* reported on an energy barrier at the ITO/TiOx interface due to traps distributed in the bulk of the TiOx layer[25], whereas Trost *et al.* showed that for atomic layer deposited TiO_x, the interface adjacent to the organic layer is the origin of the UV-light-activation effect[26]. Strikingly, the s-shape characteristics and thus UV-light-soaking effect have been shown to appear for a variety of TiO_x deposition method employed, thus making it a challenge of some general validity for TiO_x interlayers[26].

In this work, we introduce sputter-processed TiO_x interlayers possessing structural and electronic properties that result in high performance organic solar cells. Importantly, the prepared TiO_x based organic solar cells are free of initial s-shape characteristics, without introducing any surface functionalization of the TiO_x layer, and thus result in high initial fill-factor values. We show that the crystalline sputtered TiO_x layers result in power conversion efficiency values of up to 7.5% for a blend of PTB7 and $PC_{70}BM$ as the active layer, which is close to the maximum achievable efficiency for the PTB7: $PC_{70}BM$ material system. In addition, we report on the effect of different TiO_x deposition temperatures on the organic solar cell device performance, and investigate the crystallographic phase and surface morphology of the TiO_x layers for the various growth temperatures leading to the OPV performance trends. Finally, ultra-violet photoelectron spectroscopy (UPS) studies were conducted to probe the work function as well as valence band

position, and X-ray photoelectron spectroscopy (XPS) were employed to characterize the thin film composition. Our study thus presents TiO_x electron transport layers for OPV that does not require light soaking, and still allows for the use of relatively low temperature fabrication processes of around 150°C.

RESULTS AND DISCUSSION. Organic solar cells having the device configuration of ITO/TiO_x(40 nm)/PTB7: $PC_{70}BM$/MoO_3(8 nm)/Ag(100 nm), see figure 1a, were investigated in this study. The transmission spectra of the TiO_x thin film deposited on ITO substrates at different temperatures are shown in figure 1b. The relatively high optical transmittance in the visible range is obtained for all sputter deposited TiO_x films.

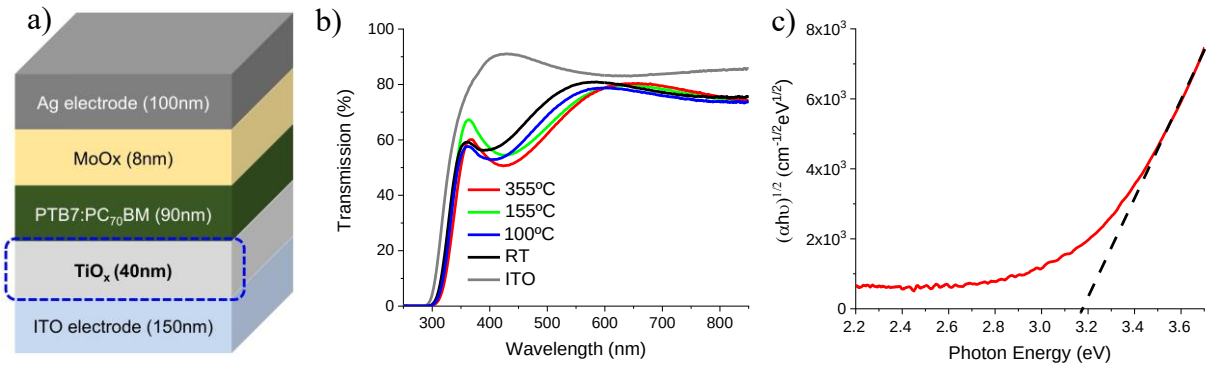

Figure 1: a: The inverted solar cell structure: ITO/TiO_x (40 nm)/PTB7: $PC_{70}BM$ / MoO_3 (8 nm)/Ag (100 nm) employed in this work. b: Transmission spectra of 40 nm TiO_x grown at different substrate temperatures on glass/ITO. The reference spectrum for glass/ITO is also shown. c) Representative Tauc plot (fitted between 3.5 – 3.7 eV) resulting in an extracted band gap energy of approx. 3.2 eV for the 355°C TiO_x layer, similar to previously reported value for anatase TiO_x[27].

By measuring the transmission and reflection spectra as well as the thickness of the films on the ITO substrate, and correcting for substrate effects, the optical absorption coefficient (α) of the TiO_x films can be determined. The band gap is then calculated using the following relation:

$$\alpha = \frac{\beta}{h\vartheta}(h\vartheta - E_g)^n,$$

where β is a band tailing parameter, E_g is the optical band gap energy, h is Planks constant and n is the transition mode power factor, which depends on the nature of the material (direct vs. indirect bandgap). Plotting of $(\alpha hv)^{1/n}$ versus hv, i.e. the Tauc plot, considering $n = 2$ typically used for anatase titanium oxide films (indirect bandgap structure) thus provides the band gap energy. As shown in figure 1c, the optical band gap was found to be around 3.2 eV for the 355°C prepared TiO_x films, which is similar to the band gap of 3.2 eV reported by Tang et al. for anatase TiO_x thin films[27]. The solar cell performance parameters of the OPV devices based on the sputtered TiO_x ETL are listed in table 1, and representative J-V characteristics for OPV devices made from different growth temperatures of the TiO_x layers are shown in figure 2. The short-circuit current densities (J_{sc}) calculated from the external quantum efficiency (EQE) spectra, figure S1, for OPV cells prepared by TiO_x (355°C) and TiO_x (155°C) are 15.9 mA/cm^2, which is in good agreement with the J_{sc} extracted from the *J-V* characteristics.

Table 1: PTB7:$PC_{70}BM$ organic solar cell performance parameters using TiO_x as ETL interlayer. The values shown are average values based on eight cells for each of the investigated interlayers. The TiO_x thin films were grown at different substrate temperatures. Reference devices using standard ZnO ETL is also shown.

Temperature (°C)	V_{oc}(V)	J_{sc} (mA/cm^2)	FF (%)	PCE (%)
355	0.73 ± 0.01	15.7 ± 1.0	60.3 ± 2.0	6.8 ± 0.6
255	0.72 ± 0.02	13.8 ± 0.6	59.6 ± 3.0	5.7 ± 0.6
205	0.71 ± 0.01	14.0 ± 0.7	60.7 ± 2.0	6.0 ± 0.5
155	0.73 ± 0.01	15.5 ± 1.0	61.4 ± 3.0	6.5 ± 0.3
100	0.70 ± 0.02	12.1 ± 1.2	52.6 ± 2.9	4.5 ± 0.4
RT	Not working devices			
ZnO reference	0.74 ± 0.01	15.1 ± 0.2	70.5 ± 2.5	7.8 ± 0.4

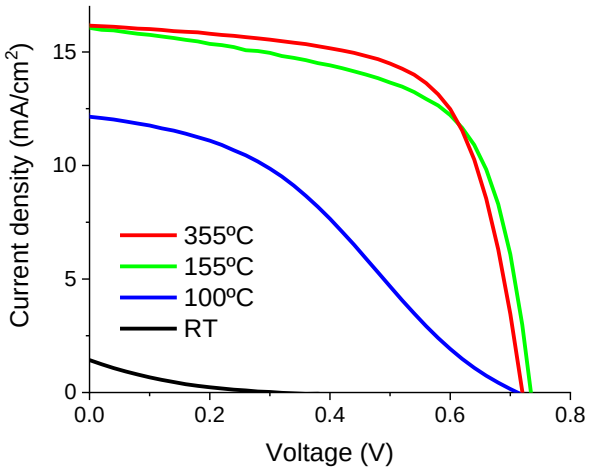

Figure 2: The J-V characteristics of representative organic solar cells for different TiO_x substrate growth temperatures.

Devices prepared at room temperature show only non-functioning cells. At TiO_x substrate temperatures of 100°C, devices start to work, however, with the well-known s-shape characteristics typically seen for TiO_x ETL layers, and a limited J_{sc} value compared to reference values for PTB7:$PC_{70}BM$ solar cells. At 155°C, however, the s-shape curve is no longer present at the initial *J-V* scan, and well-functioning devices are seen without any light soaking of the cells. The improvements arise mainly in the FF and slightly in J_{sc} parameters, as they are directly affected by the otherwise formed s-shape. When increasing the temperature further, small variations occur, but at 355°C, the performance resembles that of the 155°C devices, leading to an average device efficiency of 6.8% with 7.65% for the best performing cell. The maximum performance cell for the ZnO reference devices was 8.12%, see Suppl. Information for further details. We note that although the TiO_x based cells are relatively close in performance to the ZnO reference cells, the TiO_x cells suffer from lower FF and slightly lower V_{oc}, which could be indicative of some additional interface recombination effects taking place in these cells.

In order to understand these promising device results, structural analyses in terms of atomic force microscopy (AFM) and x-ray diffraction (XRD) investigations were made. The film surface morphology on glass/ITO substrates were characterized by AFM, see figure 3. The root mean square (RMS) roughness of the TiO_x films grown at elevated substrate temperatures was found to be homogeneous at around 4 nm, with only a minor substrate-temperature dependency.

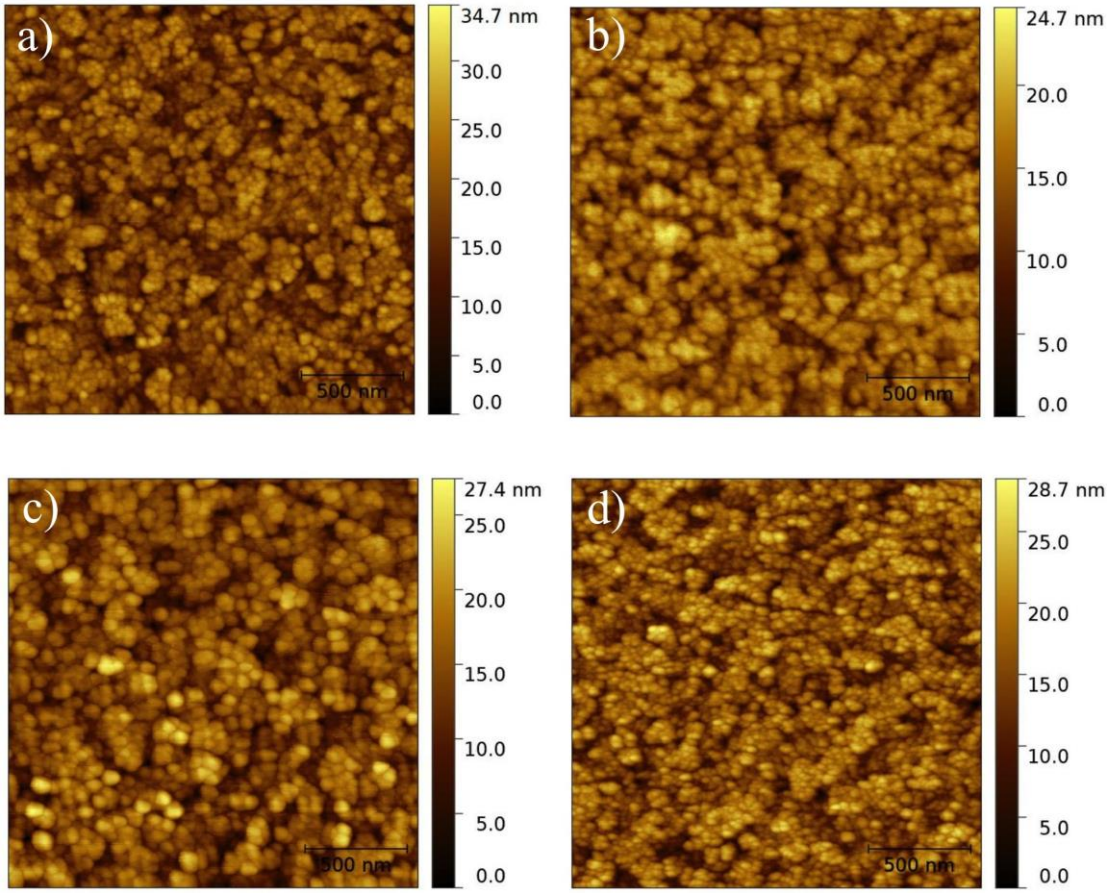

Figure 3: AFM images (2 µm x 2 µm) of the TiO_x thin films (40 nm) grown at the different substrate tempratures of: a) 155°C, b) 205°C, c) 255°C and d) 355°C.

Anatase and rutile crystalline phases are the main polymorphs for TiO_2. For TiO_x prepared by various synthesis methods, it has been shown that the initial crystalline phase that generally forms is anatase, and that the metastable anatase phase transforms to stable rutile phase at higher temperatures[28]. The transition temperatures between the different phases depend on the

concentration of doping, as previously demonstrated[29-30]. The XRD measurements of the 40 nm TiO_x layers sputtered on ITO at different temperature are shown in figure 4.

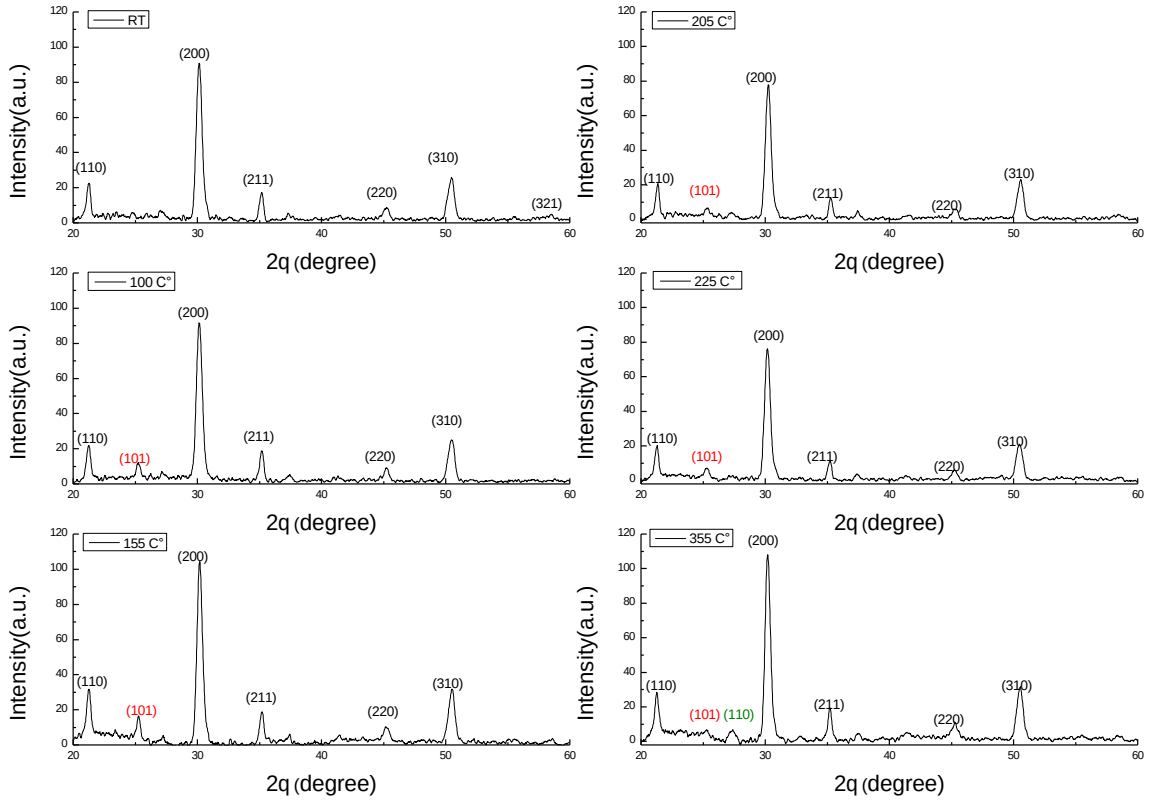

Figure 4: X-ray diffraction spectra of TiO_x films sputtered at different substrate growth temperatures.

TiO_x grown at room temperature shows amorphous characteristics. When increasing the temperature to 100°C, the anatase TiO_x (101) peak appears (marked in red). A further increase of the temperature to 355°C results in mixed anatase (101) and rutile (110) crystalline phases for the TiO_x layers, marked in red and green, repectively. The remaining peaks (marked in black) arise from the ITO substrate.

At room temperature, the sputtered TiO_x films show no diffraction peaks arising from the titanium oxide layer, demonstrating that the sputtered film is amorphous or slightly polycrystalline (below the XRD detection limit). The TiO_x diffraction peak at 25.24° (marked in red on figure 4) arising for the substrate temperatures of 100°C, 155°C, 205°C and 255°C corresponds to the anatase (101) crystal plane[30]. When increasing the temperature to 355°C, the

rutile crystal plane of (110) appears (marked in green on figure 4)[32]. All other diffraction peaks observed in the spectra originate from the ITO layer. The reflection from the (200) crystalline plane resulted in the characteristic peak at 2θ =30.18°, which is close to the reference ITO peak (2θ =30.58°)[32].

Clearly, a strong correlation between the appearances of crystalline phases in the TiO_x layers and the device performance is observed. Similar trends have recently been demonstrated for sputtered molybdenum oxide films, used as hole contacts in organic photovoltaic devices, and was attributed to modified work function and transport properties upon crystallization of the material[33-36]. The crystallization was shown to take place for super-oxidized metal oxide films, i.e. films that possess an excess amount of oxygen during the sputtering process[35-36]. For the TiO_x films developed as OPV electron selective contacts in this work, the XRD peaks arise at the point where the devices start functioning, and close to where the s-shape characteristics disappear, namely for TiO_x substrate temperatures of 100-155°C. In order to elaborate further on this, we investigated the TiO_x layers with photoelectron spectroscopy measurements.

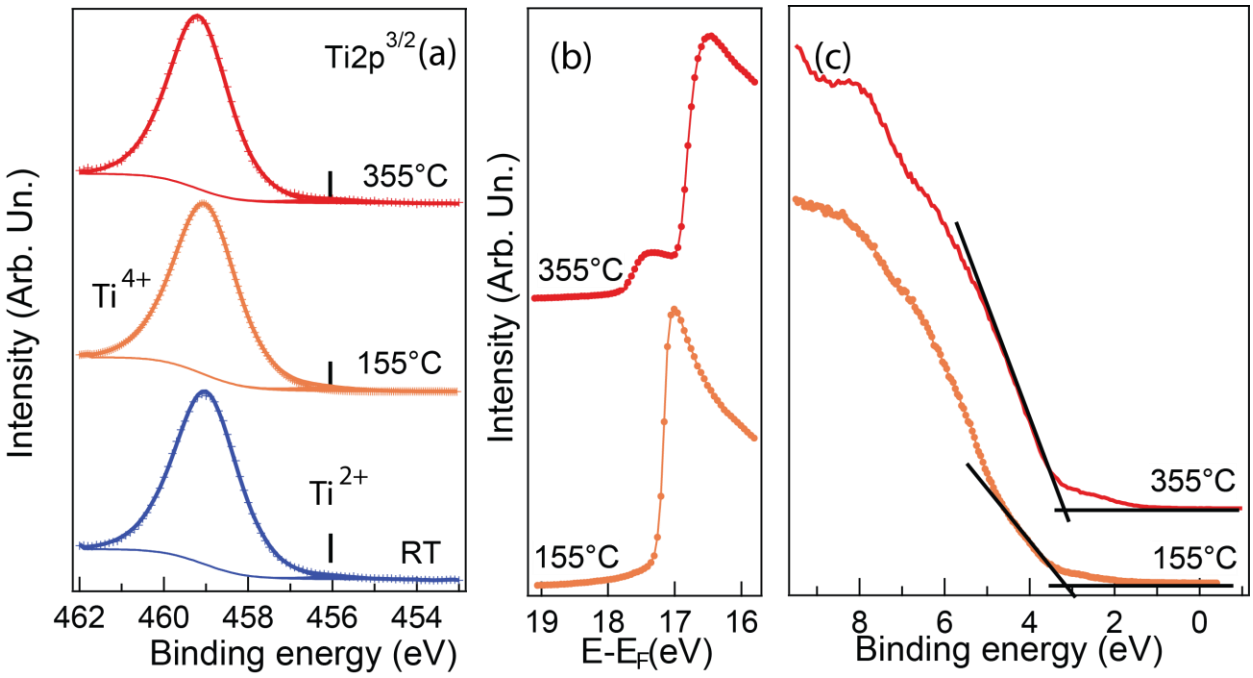

Figure 5: (a) XPS of Ti2p3/2 of RT sputtered TiO_x, 155°C sputtered TiO_x, 355°C sputtered TiO_x, (b) Secondary electron cut-off spectrum of the 155°C and 355°C sputtered TiO_x film, annealed before the UPS measurement, and (c) Valence band spectrum of the 155°C and 355°C sputtered TiO_x film after annealing.

Fig. 5 displays XPS measurements of the RT, 155°C and 355°C sputtered sample (Fig. 5a) and secondary electron cut-off and valence band on the 155°C and 355°C sputtered samples (Fig. 5b and 5c). In order to remove residual surface contaminations on the sputtered samples at 155°C and 355°C, annealing prior to valence band and secondary electron cut-off measurements at about 150°C and 250°C, respectively, has been conducted. The composition of the TiO_x layer for the 355°C sputtered sample, post-annealed at 250°C, is evaluated to be $x=2.2 \pm 0.1$ (see Suppl. Information). This finding shows that the composition of the high temperature sputtered oxide remains nearly stoichiometric or even slightly super-oxidized, also following the post-annealing process.

In Fig. 5a, the $Ti2p^{3/2}$ is found at a binding energy of 459.18 eV for the 355°C sputtered sample spectrum, and at 459.0 eV for the 155°C and RT sputtered sample spectrum, corresponding to a Ti^{4+} oxidation state as shown e.g. by Kashiwaya et. al[37]. The small energy shift may arise from slight differences in the electron chemical potential for the two preparations, following a very comprehensive study from Greiner et al.[38] on transition metal oxides. To elaborate the analysis, both spectra have been decomposed using Gaussian-Lorentzian functions to fit experimental XPS spectra using Shirley background (See Suppl. Information for details on analysis). The best agreement is obtained with the introduction of an additional component around 456.1 eV for all samples, corresponding to Ti^{2+} contributions (i.e. TiO species) separated by about 3 eV from the Ti^{4+} component[39]. The Ti^{2+} component represents respectively 1.3 % - 2.1 % - 2.5 % of $Ti2p^{3/2}$ intensity for the RT – 155°C - 355°C sputtered samples. This indicates a slight reduction of the TiO_x thin films upon annealing, as also seen for post-annealed crystallization of sputtered, super-oxidized molybdenum oxide layers[35].

In figure 5, the secondary electron cut-off spectrum (b) and valence-band region (c) have been recorded for the 155°C and 355°C sputtered samples, which display a sharp cut-off attributed to the TiO_x layer, corresponding to work functions of 4.0 eV and 4.20 eV, respectively. It should be noted that the sample presents small contamination of residual carbon even after the post-annealing procedure, which potentially underestimates slightly the work function[40], the contamination being greater for 155°C sputtered sample due to the limited post-annealing temperature. The pre-edge feature, visible for the 355°C sputtered sample, is a signature of the ITO substrate that is surrounding the TiO_X layers. Our finding is in-line with work functions obtained on TiO_x films presenting oxygen vacancies. From the spectra displayed in Fig. 5c, the position of the valence band can be extracted by extrapolating the slope of photoemission edge to

zero intensity. The corresponding value obtained is 3.1+/-0.1 eV for both samples, which is close to valence band positions found in the literature[38].

From the XPS and UPS investigations it is demonstrated that the sputtered films prepared at 155°C and 355°C possess very similar electronic structure, and that the high temperature sputtered sample remains nearly stoichiometric, or even slightly super-oxidized, and that a low density of oxygen-deficient defect states appear upon crystallization of the films. This is similar to recently reported sputtered molybdenum oxide layers, where improved OPV device performances were also seen upon crystallization of the super-oxidized films[36]. As noted previously, the s-shape curve appearing for titanium oxide OPV devices is due to negatively charged chemisorbed oxygen, forming defect states in the band gap of the oxide[25-26]. The charged oxygen species have shown to lead to upward band bending in the oxide, as well as to downward band bending in an interfaced organic electron acceptor layer[26], and thus an energy barrier for charge extraction at that interface. Although the band alignment to the organic PCBM layer should be investigated to fully understand the origin of the s-shape free characteristics observed, the electronic energy scheme presented, displaying a relatively low TiO_x work function value (4.0 eV - 4.2 eV) and a valence band position (3.1 eV) and E_g value (3.2 eV) that places the Fermi level close to TiO_x conduction band, resembles that previously reported on for TiO_x[25] and ETL metal oxide layer[26] with low trap and defect densities. It can thus be assumed that the crystalline TiO_x layers formed from the sputtering process demonstrate a low density of surface defects and traps, otherwise leading to the well-known s-shape characteristics.

CONCLUSIONS. In this work, we have introduced sputtered titanium oxide layers as efficient electron selective contact layers in organic solar cell devices. The composition of the sputtered TiO_x layers is $x=2.2 \pm 0.1$ (analyzed for the 355°C prepared sample post-annealed), and

crystallization during growth at elevated substrate temperatures is demonstrated, starting as low as 100°C. Strikingly, upon further crystallization of the TiO_x layer, s-shape free device characteristics are seen, which is otherwise known to be a typical problem for pure TiO_x interlayers in OPV devices. Combined optical, structural, compositional and electronic energy level investigations of the TiO_x layers grown at different surface temperatures reveal the electronic energy level scheme for the TiO_x layers, as well as the temperature onset for the crystallization process resulting in the appealing device properties. The PTB7:$PC_{70}BM$ OPV devices show PCE values of up to 7.65% using the sputtered TiO_x contact layers, which is relatively close to the PCE of reference ZnO based cells (max at 8.12%). However, lower FF and slightly lower V_{oc} values are still seen in these TiO_x based cells, which could be indicative of some additional interface recombination effects. Importantly though, at 155°C TiO_x growth temperature well-functioning OPV devices are developed, making it a relatively low temperature fabrication process.

ACKNOWLEDGEMENTS. M.M. acknowledges Danmarks Frie Forskningsfond, DFF FTP for funding of the project React-PV, No. 8022-00389B. The research leading to these results has received funding from the People Programme (Marie Curie Actions) of the European Union's Seventh Framework Programme FP7/ 2007-2013/under REA Grant Agreement No. 607232, THINFACE. PJ, HL, JL, BJ, PB, M.Mi, M.M, acknowledge the Innovation Fund Denmark for support of the 'SunTune' project.

AUTHOR INFORMATION

Corresponding Author

*madsen@mci.sdu.dk

EXPERIMENTAL SECTION. *TiOx preparation by RF magnetron sputtering:* The TiO_x thin films were fabricated in a 13.56 MHz rf-MS system from AJA ATC Orion system. The sputtering was performed in confocal geometry with the target-substrate distance fixed at 10 cm and the tilt angle of the magnetron at 10°. The substrates were placed horizontally in a substrate holder having a rotation feature to ensure uniform film deposition. The vertical and horizontal positions of the center of the substrate holder with respect to the target are 9.8 cm and 1.7 cm, respectively. The sputtering target used in this work was 99.99 % pure TiO_2 ceramic target of 5 cm in diameter (from Able Target Limited). The substrates used in this work were ITO coated glass substrates, BOROFLOAT® 33 glass substrates and c-Si wafers. The substrates were cleaned consecutively in ultrasonic bath for 10 min using acetone, isopropanol, and deionized water, and completely dried out with N_2 gas followed by baking at 100 °C in an oven for 1 hour, to ensure complete dryness prior to deposition. The base pressure of the system was typically maintained in the range of 10^{-7} mTorr prior to the deposition. A mixed gas flow of Ar (99.999%):13 sccm and O_2 (99.9999%):0.25 sccm was used. The rf power was kept constant at 100 W and the plasma pressure during the deposition was fixed at 3 mTorr.

Device fabrication: Blends of the active layer PTB7: $PC_{70}BM$ (purchased from 1-material and Solenne) were spin coated at 1000 rpm for 2 minutes on top of ITO substrates (Lumtec, sheet resistance of 9-15 Ω/sq) covered with 40 nm of sputter deposited TiO_x thin film and dried out in a slight vacuum (10^{-1} mbar) for 20 min. The blend of PTB7:$PC_{70}BM$ was prepared by dissolving PTB7 and $PC_{70}BM$ in a weight ratio of 1:1.5 in chlorobenzene, and subsequently adding small amount (3 % v/v) of 1, 8-diiodooctane (DIO) additive to the solution. The solution was stirred overnight at room temperature. Finally, 8 nm of MoO_3 and 100 nm of Ag were thermally

evaporated (without an intermediate vacuum break) with the growth rate of 0.02 nm s^{-1} and 0.05 nm s^{-1} at 5×10^{-7} mbar on the active layer, respectively.

External quantum efficiency was measured using a 150 W Xenon lamp connected to a monochromator (VIS-NIR Newport Cornerstone 1/4m), which was connected to a microscope (Mitoyo FS-70) by an optical fiber. The measurement was carried out in air at room temperature, at the wavelength range from 300 nm to 800 nm. A certified silicon photodiode (Hamamatsu S2386-44 K) was used for calibration at each wavelength.

J-V characteristics were measured using a solar simulator (class AAA, Sun 3000, Abet Technologies Inc., USA) with the lamp intensity of 100 $mWcm^{-2}$, which closely resembles the AM1.5 spectrum. The solar cells were characterized under dark and illumination by applying voltage sweeps of -1 V to 1 V. For this purpose, a 2400 source measure unit (Keithley Instruments Inc., USA) was used.

Surface morphology images were obtained using atomic force microscope (Veeco Dimention 3100) in tapping mode.

XRD..

Optical transmittance measurements were carried out using an UV-VIS-IR spectrophotometer with an integrated sphere attachment (SHIMADZU-UV2700).

Photoemission spectra (core levels, valence band and secondary electron cut-off) have been measured at Institut des NanoSciences de Paris on a hemispherical photoemission spectrometer (EA 125 Omicron) using ultraviolet He I ($h\nu$ = 21.2 eV) excitation, UPS, and AlK-α ($h\nu$ = 1486.6 eV), XPS, with an overall resolution around 0.1 eV. Experiments have been carried out on the 40 nm TiO_x layers sputtered on ITO at 355°C and 155°C, and annealed to 250°C and

150°C, respectively, prior to UPS measurement in a preparation chamber connected to the analysis chamber, in order to remove carbon contamination arising from atmosphere exposure. The secondary electron cut-off spectrum has been obtained by applying a negative bias of -10V on the sample and spectra are plotted relatively to the Fermi energy. The work function was calculated by extrapolating the linear part of the electron cut-off energy to zero intensity and by subtracting this energy from the photon energy (21.2 eV).

[1] Krebs, F. C.; Espinosa, N.; Hösel, M.; Søndergaard, R. R.; Jørgensen, M., "25th Anniversary Article: Rise to Power – OPV-Based Solar Parks," *Advanced Materials*, vol. 26, pp. 29-39, 2014

[2] Lucera, L.; Machui, F.; Schmidt, D.; Adams, J.; Strohm, S.; Ahmad, T.; Forberich, K.; Egelhaaf, H.-J.; Brabec, C. J., "Highly efficient, large area, roll coated flexible and rigid OPV modules with geometric fill factors up to 98.5% processed with commercially available materials," *Energy Environ. Sci*., vol. 9, pp. 89-94, 2016

[3] Berny S.; Blouin, N.; Distler, A.; Egelhaaf, H.-J.; Krompiec, M.; Lohr, A.; Lozman, O. R.; Morse, G. E.; Nanson, L.; Pron, A.; Sauermann, T.; Seidler, N.; Tierney, S.; Tiwana, P.; Wagner, M.; Wilson, H., ″Solar trees : First Large-Scale Demonstration of Fully Solution Coated, Semitransparent, Flexible Organic Photovoltaic Modules," *Adv. Sci*., vol. 3, pp. 1500342, 2015

[4] Meng, L.; Zhang, Y.; Wan, X.; Li, C.; Zhang, X.; Wang, Y.; Ke, X.; Xiao, Z.; Ding, L.; Xia, R.; Yip, H.; Cao, Y.; Chen, Y., "Organic and Solution-Processed Tandem Solar Cells with 17.3% Efficiency," *Science*, vol. 361, pp. 1094–1098, 2018

[5] Cui, Y.; Yao, H.; Zhang, J.; Zhang, T.; Wang, Y.; Hong, L.; Xian, K.; Xu, B.; Zhang, S.; Peng, J.; Wei, Z.; Gao, F.; Hou, J., "Over 16% efficiency organic photovoltaic cells enabled by a chlorinated acceptor with increased open-circuit voltages," *Nat. Commun.*, vol. 10, pp. 2515, 2019

[6] Yin, Z.; Wei, J.; Zheng, Q., "Interfacial materials for organic solar cells: Recent advances and perspectives,"*Advanced Science*, vol. 3, pp. 1500362, 2016

[7] Yin, Z.; Zheng, Q.; Chen, S.-C.; Li, J.; Cai, D.; Ma, Y.; Wei, J., "Solution-derived poly(ethylene glycol)-TiOx nanocomposite film as a universal cathode buffer layer for enhancing efficiency and stability of polymer solar cells," *Nano Res.*, vol. 8, pp. 456-468, 2015

[8] Ouyang, X.; Peng, R.; Ai, L.; Zhang, X.; Ge, Z., "Efficient polymer solar cells employing a non-conjugated small-molecule electrolyte," *Nat. Photonics*, vol. 9, pp. 520-524, 2015

[9] White, M. S.; Olson, D. C.; Shaheen, S. E.; Kopidakis, N.; Ginley, D. S., "Inverted bulk-heterojunction organic photovoltaic device using a solution-derived ZnO underlayer," *Applied Physics Letters* vol. 89, pp. 143517 (2006)

[10] Waldauf, C.;Morana, M.; Denk, P.; Schilinsky, P.; Coakley, K.; Choulis, S. A., Brabec, C. J., "Highly efficient inverted organic photovoltaics using solution based titanium oxide as electron selective contact," *Applied Physics Letters*, vol. 89, pp. 233517, (2006)

[11] Siddiki, M. K.; Venkatesan, S.; Qiao, Q., "Nb_2O_5 as a new electron transport layer for double junction polymer solar cells," *Physical Chemistry Chemical Physics* , vol. 14, pp. 4682-4686, 2012.

[12] Trost, S.; Zilberberg, K.; Behrendt, A.; Riedl, T., "Room-temperature solution processed SnO_x as an electron extraction layer for inverted organic solar cells with superior thermal stability," *Journal of Materials Chemistry*, vol. 22, pp. 16224-16229, 2012

[13] Oh, H.; Krantz, J.; Litzov, I.; Stubhan, T.; Pinna, L.; Brabec, C. J., "Comparison of various sol–gel derived metal oxide layers for inverted organic solar cells," *Solar Energy Materials and Solar Cells*, vol. 95, pp. 2194-2199, 2011

[14] Yin, Z. , Zheng, Q, Chen, S.-C.; Cai, D.; Zhou, L; Zhang, J., "Bandgap Tunable $Zn_{1-x}Mg_xO$ Thin Films as Highly Transparent Cathode Buffer Layers for High-Performance Inverted Polymer Solar Cells," *Advanced Energy Materials*, vol. 4, pp. 1301404, 2014

[15] Li, X.; Xie, F.; Zhang, S.; Hou, J.; Choy, W. C. H., "Over 1.1 eV Workfunction Tuning of Cesium Intercalated Metal Oxides for Functioning as Both Electron and Hole Transport Layers in Organic Optoelectronic Devices," *Advanced Functional Materials*, vol. 24, pp. 7348-7356, 2014

[16] Schmidt H.; Zilberberg, K.; Schmale, S.; Flügge, H.; Riedl, T.; Kowalsky, W, "Transient characteristics of inverted polymer solar cells using titaniumoxide interlayers," *Applied Physics Letters*, vol. 96, pp. 243305, 2010

[17] Park, S. H.; Roy, A.; Beaupre, S.; Cho, S.; Coates, N.; Moon, J. S.*, et al.*, "Bulk heterojunction solar cells with internal quantum efficiency approaching 100%," *Nat Photon,* vol. 3, pp. 297-302, 2009

[18] Xiong, J.; Yang, B.; Zhou, C.; Yang, J.; Duan, H.; Huang, W.*, et al.*, "Enhanced efficiency and stability of polymer solar cells with TiO_2 nanoparticles buffer layer," *Organic Electronics,* vol. 15, pp. 835-843, 2014

[19] Hadipour, A.; Müller, R.; Heremans, P., "Room temperature solution-processed electron transport layer for organic solar cells," *Organic Electronics,* vol. 14, pp. 2379-2386, 2013

[20] Bao, X. C.; Sun, L.; Shen, W. F.; Yang, C. P.; Chen, W. C.; Yang, R. Q., " Facile preparation of TiO_X film as an interface material for efficient inverted polymer solar cells," *J. Mater. Chem. A*, vol. 2, pp. 1732, 2014

[21] Lin, Z.; Jiang, C.; Zhu, C.; Zhang, J., "Development of Inverted Organic Solar Cells with TiO2 Interface Layer by Using Low-Temperature Atomic Layer Deposition," *ACS Applied Materials and Interfaces*, Vol. 5, pp. 713-718, 2013

[22] G. Kim, J. Kong, J. Kim, H. Kang, H. Back, H. Kim*, et al.*, "Overcoming the Light-Soaking Problem in Inverted Polymer Solar Cells by Introducing a Heavily Doped Titanium Sub-Oxide Functional Layer," *Advanced Energy Materials,* vol. 5, pp. 1401298, 2015

[23] H. Choi, J. S. Park, E. Jeong, G.-H. Kim, B. R. Lee, S. O. Kim*, et al.*, "Combination of Titanium Oxide and a Conjugated Polyelectrolyte for High-Performance Inverted-Type Organic Optoelectronic Devices," *Advanced Materials,* vol. 23, pp. 2759-2763, 2011

[24] M. Vasilopoulou, D. G. Georgiadou, A. Soultati, N. Boukos, S. Gardelis, L. C. Palilis*, et al.*, "Atomic-Layer-Deposited Aluminum and Zirconium Oxides for Surface Passivation of TiO2 in High-Efficiency Organic Photovoltaics," *Advanced Energy Materials,* vol. 4, pp. 1400214, 2014

[25] Kim J.; Kim, G.; Choi, Y.; Lee, J.; Park, S. H.; Lee, K., ″Light-soaking issue in polymer solar cells: Photoinduced energy level alignment at the sol-gel processed metal oxide and indium tin oxide interface*," Journal of Applied Physics*, vol. 111, pp. 114511, 2012.

[26] Trost, S.; Zilberberg, K.; Behrendt, A.; Polywka, A.; Görrn, P.; Reckers, P.; Maibach , J.; Mayer, T.; Riedl, T., "Overcoming the "Light-Soaking" Issue in Inverted Organic Solar Cells by the Use of Al:ZnO Electron Extraction Layers," Advanced Energy Materials, vol. 3, pp. 1437-1444, 2013

[27] Tang, H.; Prasad, K.; Sanjinès, R.; Schmid, P. E.; Lévy, F., "Electrical and optical properties of TiO_2 anatase thin films," *Journal of Applied Physics,* vol. 75, pp. 2042-2047, 1994

[28] Hanaor, D. A. H.; Sorrell, C. C., "Review of the anatase to rutile phase transformation," *Journal of Materials Science,* vol. 46, pp. 855-874, 2011

[29] Johannsen, S. R.; Roesgaard, S.; Julsgaard, B.; Ferreira, R. A. S.; Chevallier, J.; Balling, P.; Ram, S. K.; Larsen, A. N., "Influence of TiO_2 host crystallinity on Er^{3+} light emission," *Opt. Mat. Express*, vol. 6, pp. 1664-1678, 2016

[30] Lakhotiya, H.; Christiansen, J.; Hansen, J. L.; Balling, P.; Julsgaard, B., "Upconversion luminescence from magnetron-sputtered Er^{3+}-doped TiO_2 films: Influence of deposition- and annealing temperatures and correlation to decay times," *J. Appl. Phys*., vol. 124, pp. 163105, 2018

[31] Ali, K.; Khan, S. A.; Jafri, M. Z. M., "Structural and optical properties of ITO/TiO_2 anti-reflective films for solar cell applications," *Nanoscale Research Letters,* vol. 9, pp. 175, 2014

[32] Kuo-Tong L.; Jenn-Ming, W., "Rf-Magnetron Sputtering of Titanium Dioxide for Microelectronic Applications," *Japanese Journal of Applied Physics,* vol. 43, p. 232, 2004

[33] Cauduro, A. L. F.; Fabrim, Z. E.; Ahmadpour, M.; Fichtner, P. F. P.; Hassing, S.; Rubahn, H.-G.; Madsen, M, "Tuning the optoelectronic properties of amourphous MoOx films by reactive sputtering," *Applied Physics Letters*, vol. 106, pp. 202101, 2015

[34] Cauduro, A. L. F., dos Reis, R.; Chen, G.; Schmid, A. K.; Rubahn, H.-G.; Madsen, M., "Work Function Mapping of MoO_x Thin-Films for Application in Electronic Devices," *Ultramicroscopy,*

vol. 183, pp. 99, 2017

[35] Cauduro, A. L. F.; dos Reis, R.; Chen, G.; Schmid, A. K.; Méthivier, C.; Rubahn, H.-G.; Bossard-Giannesini, L.; Cruguel, H.; Witkowski, N.; Madsen, M., "Crystalline Molybdenum Oxide Thin-Films for Application as Interfacial Layers in Optoelectronic Devices," *ACS Applied Materials and Interfaces*, vol. 9, pp. 7717, 2017

[36] Ahmadpour, M.; Cauduro, A. L. F.; Méthivier, C.; Kunert, B.; Resel, R.; Turkovic, V.; Rubahn, H.-G.; Witkowski, N.; Schmid, A. K.; Madsen, M., "Crystalline molybdenum oxide layers as efficient and stable hole contacts in organic photovoltaic devices," *ACS Applied Energy Materials*, vol. 2, pp. 420-427, 2019

[37] Kashiwaya, S.; Morasch, J.; Streibel, V.; Toupance, T.; Jaegermann, W.; Klein, A., "The Work Function of TiO_2," *Surfaces*, vol. 1, pp. 73-89, 2018

[38] Greiner, M. T.; Chai, L.; Helander, M. G.; Tang, W. M.; Lu, Z. H., "Transition Metal Oxide Work Functions: The Influence of Cation Oxidation State and Oxygen Vacancies," *Advanced Functional Materials*, vol. 22, pp. 4557–4568, 2012

[39] Biesinger, M. C.; Lau, L. W. M.; Gerson, A. R.; Smart, R. St. C., "Resolving Surface Chemical States in XPS Analysis of First Row Transition Metals, Oxides and Hydroxides: Sc, Ti, V, Cu and Zn," Applied Surface Science, vol. 257, pp. 887, 2010

[40] Greiner, M. T.; Helander, M. G.; Wang, Z.-B.; Tang, W.-M.; Lu, Z.-H., "Effects of Processing Conditions on the Work Function and Energy-Level Alignment of NiO Thin Films," *Journal of Physical Chemistry C*, vol. 114, pp. 19777, 2010